Ethylene Glycol Co-Solvent Enables Stable Aqueous Ammonium-Ion Batteries with Diluted Electrolyte

Huifang Fei, Fuhua Yang,* Zenonas Jusys, Stefano Passerini, and Alberto Varzi*

Aqueous ammonium-ion batteries (AAIBs) are considered as one of the most promising technologies for large scale energy storage applications, due to their intrinsic safety, environmental friendliness and low cost. Nevertheless, the practical application of AAIBs is impeded by hydrogen evolution reaction (HER) occurring in diluted aqueous electrolyte. Highly concentrated electrolytes can improve electrochemical stability but lead to higher costs and increased hydrolysis of NH_4^+. In this work ethylene glycol (EG) is proposed as co-solvent, which can act as H-bond modulating agent, to increase the stability of AAIBs with diluted electrolytes. The perturbation of water H-bond network regulated by EG is proved by spectroscopic methods, while the suppressed HER is confirmed by differential electrochemical mass spectrometry (DEMS) results. As a result, full cells with 3,4,9,10-perylenebis(dicarboximide) (PTCDI) anode and FeFe(CN)$_6$ (FeHCF) cathode and EG-added electrolyte exhibit stable cycling performance with capacity retention of 77% after 1950 cycles.

1. Introduction

Aqueous batteries are emerging as potential low-cost alternative to the state-of-the-art lithium-ion systems for energy storage applications at various scales (e.g., house-, industry- and grid-scale), in which the top priority is reducing manufacturing and operating costs rather than maximizing volumetric and gravimetric energy. In fact, the aqueous electrolyte provides intrinsic advantages such as high safety, low-cost and environmental friendliness.[1] Multiple aqueous battery chemistries based on both metallic (Li^+, Na^+, K^+, Zn^{2+}, and Al^{3+}, et ct.).[1,2] and non-metallic ion carriers (H^+ and NH_4^+).[3] have been demonstrated. Research on ammonium-ion batteries has recently gained
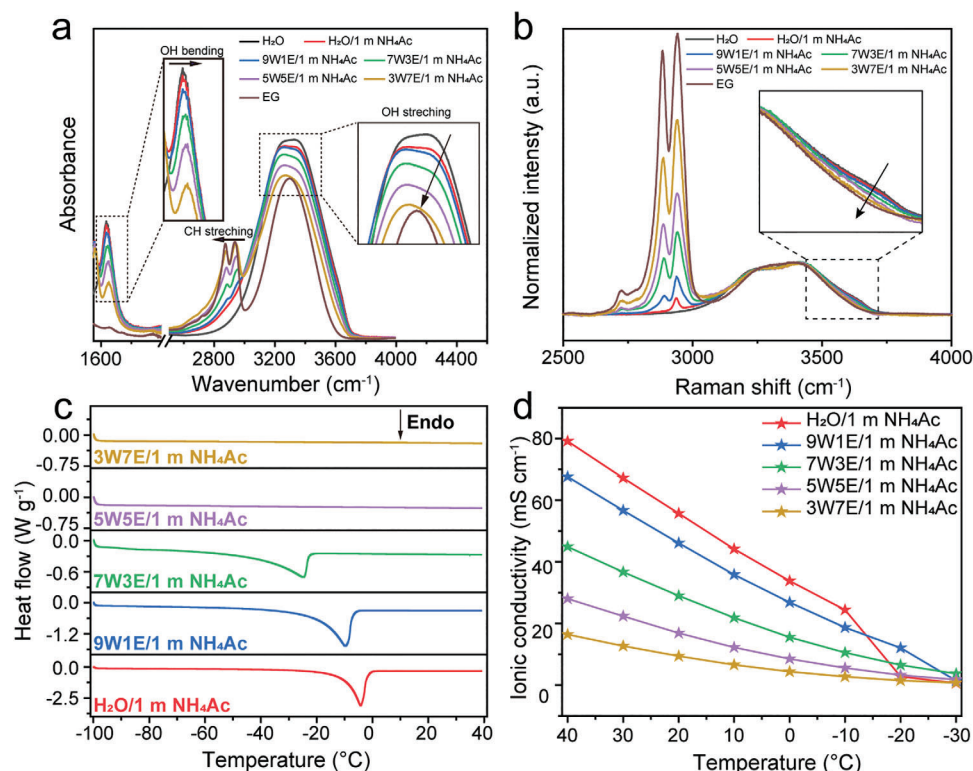
H. Fei, F. Yang, Z. Jusys, S. Passerini, A. Varzi
Helmholtz Institute Ulm (HIU)
Helmholtzstrasse 11, 89081 Ulm, Germany
E-mail: fuhua.yang@kit.edu; alberto.varzi@kit.edu
H. Fei, F. Yang, Z. Jusys, S. Passerini, A. Varzi
Karlsruhe Institute of Technology (KIT)
76021 Karlsruhe, Germany

© 2024 The Authors. Advanced Functional Materials published by Wiley-VCH GmbH. This is an open access article under the terms of the Creative Commons Attribution-NonCommercial License, which permits use, distribution and reproduction in any medium, provided the original work is properly cited and is not used for commercial purposes.

momentum, mostly motivated by the low molar mass (18 g mol^{-1}) and small hydrated ion size (3.31 Å) of NH_4^+, which promise fast electrode kinetics and ion transport in the electrolyte.[3b,4] Analogously to other aqueous batteries, however, widening the electrochemical stability window (ESW) of the electrolyte is needed to maximize energy density and cycle life.[5] The Hydrogen Evolution Reaction (HER), resulting from reduction of water at the negative electrode, is one of the main challenges, limiting the choice of electrode materials and leading to inferior electrochemical performance and short cycle life.[6]

Identifying the correct electrolyte formulation is a key step toward suppressing HER and boosting the AAIBs performance. Using concentrated electrolytic solutions such as water-in-salt electrolytes (WiSE) represents one of the most effective strategies to minimize HER.[6a,7] In such electrolyte systems, the high salt concentration helps disrupting the H-bond network of water and the majority of water molecules in WiSE are confined in the hydration shell of the cation[8] and, therefore, less free-water is available. Since proton diffusion occurs between neighboring water molecules via the Grothus mechanism,[9] such limited amount of free water and larger separation between neighboring water molecules leads to an electrolyte with extended stability window. Jin et al. reported a 5.8 m $(NH_4)_2SO_4$ electrolyte providing an ESW of 2.39 V, which is largely improved compared to the 1.34 V of its diluted counterpart.[6a] The AAIB full cell featuring ammonium copper hexacyanoferrate and PTCDI as cathode and anode, respectively, presented remarkable cycling performance in such a concentrated electrolyte. To further increase salt concentration, highly soluble salts were also studied such as NH_4Ac and NH_4OTf.[7b,10] However, in 25 m NH_4Ac severe NH_4^+ hydrolysis was found to worsen the cathodic stability of the electrolyte.[7b] Similarly, 25 m NH_4OTf has a pH lower than 1 m NH_4OTf (3.35 and 5.73, respectively) ascribed to the NH_4^+ hydrolysis. Such a low pH is deleterious for the cycling stability of AAIBs.[4b,10] Furthermore, WiSE suffer from practical drawbacks such as high viscosity, higher cost, and, potentially, risk of salt precipitation.[11] Another major strategy to suppress HER involves the use of electrolyte additives.[12] These are expected to form H-bonds with water molecules to interrupt the continuous H-bond network of water.[13] For example, water decomposition was inhibited via the H-bond network modulation induced adding 5 m sucrose in 2 m NH_4OTf electrolyte.[10] Nevertheless,

**ADVANCED
SCIENCE NEWS**

www.advancedsciencenews.com

**ADVANCED
FUNCTIONAL
MATERIALS**

www.afm-journal.de

Figure 1. Physical characterizations of the aqueous-EG hybrid electrolytes with varying water:EG volume ratio. a) FTIR and b) Raman spectra of the electrolytes, including pure water and EG as reference. c) Differential Scanning Calorimetry (DSC) curves highlighting the melting behavior of the different electrolytes upon heating. d) Ionic conductivity of the electrolytes in the −30 to 40 °C temperature range.

the additive led to a decrease of ionic conductivity of the electrolyte from 68.7 to 3.1 mS cm^{-1}. More efficient strategies need to be developed in order to improve the electrolyte stability without excessively sacrificing other important properties such as ionic conductivity.

Ethylene glycol (EG) as H-bond modulator and/or antifreeze agent has been already studied in aqueous metallic ion batteries (e.g., Zn^{2+} and Li$^+$).[14] However, no systematic study has been performed so far about the impact of EG in ammonium-ion battery electrolytes. Therefore, in this work we explore EG as co-solvent to disrupt the H-bond network in diluted ammonium acetate electrolytes with the aim of minimizing HER and improving AAIBs performance. The physico-chemical properties and HER behavior of the electrolytes with various EG volume ratios were systematically investigated. Notably, full ammonium-ion cells composed of FeHCF cathode and PTCDI anode with optimized electrolyte (H$_2$O:EG = 5:5, volume ratio) showed improved electrochemical performance due to the inhibited side reactions such as i) HER, ii) Al corrosion and iii) dissolution of FeHCF.

2. Results and Discussion

To investigate the impact of EG on the physico-chemical properties of ammonium acetate electrolytes, a series of hybrid electrolytes was prepared, where the EG volume ratio was increased from 0% to 10%, 30%, 50%, and 70%. The samples were labeled as H$_2$O, 9W1E, 7W3E, 5W5E, and 3W7E, respectively. The concentration of the ammonium acetate was maintained constant

at 1 mol kg^{-1} (1 m), considering the total solvent mass, i.e., water and EG. Fourier Transform Infrared spectroscopy (FTIR) and Raman spectroscopy were employed to study the H-bond network evolution upon addition of EG in the aqueous electrolytes. As evidenced by the FTIR spectra shown in **Figure 1a**, the OH stretching vibration (3000–3500 cm^{-1}) undergoes an evident red shift while the OH bending (1600–1700 cm^{-1}) vibration shows a blue shift with the increase of EG content, indicating interaction between EG and water molecules, in agreement with previous reports.[15] Figure 1b presents the Raman spectra of various electrolytes and solvents in the range of 2500–4000 cm^{-1}. The O—H stretching feature is located between 3000 and 3750 cm^{-1}. The small bump of H$_2$O and H$_2$O/1 m NH$_4$Ac at high wavenumber (enlarged graph) is ascribed to the O—H stretching vibration of free water (Raman peaks located at 3627 cm^{-1}).[16] The bump became smaller to disappeared when increasing the EG volume ratio from 10% (9W1E) to 70% (3W7E), suggesting that the fraction of free O–H is reduced with the addition of EG. The H-bond network was further studied by deconvoluting the O—H stretching band of water molecules into three peaks, as shown in Figure S1 (Supporting Information). The three peaks are related to strong, weak, and non-H-bonds of water in different electrolytes and their ratio was also calculated.[17] The peak related to non-H-bonds decreased with increasing EG, while the one related to weak H-bonds showed the opposite trend. Notably, non-H-bonds disappeared when the EG volume ratio exceeded 30%. Moreover, the strong H-bonds kept decreasing as EG volume ratio increased. To gain further information on hydrogen bonds,

**ADVANCED
SCIENCE NEWS**

www.advancedsciencenews.com

**ADVANCED
FUNCTIONAL
MATERIALS**

www.afm-journal.de

the OH signal in the ^{1}H nuclear magnetic resonance (NMR) spectra of the solvents and electrolytes were collected. As shown in Figure S2 (Supporting Information), the protons in pure water resonate at ≈3.45 ppm, while the water protons have a downfield shift of ca. 3.50 ppm in H_2O/1 m NH_4Ac. This result shows that the electron density of ^{1}H from H_2O decreases after dissolving NH_4Ac, which indicates the interaction of protons in NH_4^+ with the O atom of H_2O.[15a,17] As the EG increases from 10% to 70%, the chemical shift of ^{1}H from H_2O in the hybrid electrolytes continually moves to lower field with a larger σ and the peaks become broader. The larger σ may result from the interactions between protons of OH in EG and O from water, further confirming the perturbation of the H-bond network by EG addition. Additionally, the broader peaks are attributed to disorder and residual dipole coupling of different species, which are merged.[18] The 1H resonances from OH in pure EG is at 4.44 ppm.

Differential Scanning Calorimetry (DSC) was also carried out to further verify the perturbation of the H-bond network by EG addition (Figure 1c). The melting temperature (T_m) of the electrolytes was obtained by tracking the heat flow upon heating up from to −100 to 40 °C. As expected, T_m decreased as the volume ratio increased from 0% to 30%. For EG volume ratios higher than 50% no melting point could be observed, indicating the outstanding freezing resistance of the EG-rich electrolytes. In fact, EG is notoriously used as anti-freezing agent and deicer.[19] From the above-mentioned measurements, it can be concluded that introducing EG into aqueous 1 m NH_4Ac electrolytes the water H-bond network is largely disrupted, resulting on a much wider liquid phase temperature range. To understand the impact on ionic transport, the ionic conductivity of the electrolytes was determined as function of temperature (see Figure 1d). For better comparison, the values obtained at 20 °C are summarized in Figure S3 (Supporting Information). The ionic conductivity decreased from 57.9 to 9.1 mS cm^{-1} when increasing the EG volume ratio from 0 (H_2O/1 m NH_4Ac) to 70% (3W7E), while the water-free EG/1 m NH_4Ac electrolyte showed negligible conductivity of only 3.4×10^{-4} mS cm^{-1}. At lower temperatures, H_2O/1 m NH_4Ac suffers from a sudden conductivity drop below −10 °C, which agrees with the DSC results. Although the values for all samples decreased below 0 °C, the 9W1E and 3W7E still provided a remarkable conductivity of 12.0 and 6.5 mS cm^{-1}, respectively, at −20 °C. Moreover, the addition of EG substantially reduced the volatility of the electrolyte, also acting as an anti-freezing agent at sub-zero temperatures (see the abrupt decrease in conductivity at low temperatures for the EG-free electrolyte, Figure 1d). As shown in Figure S4 (Supporting Information), after 7 days storage in open glass vials at 20 ± 2 °C the weight retention of 5W5E/1 m NH_4Ac (67%) was even superior to that of the highly concentrated H_2O/10 m NH_4Ac electrolyte (61%). The bare diluted H_2O/1 m NH_4Ac electrolyte evaporated almost entirely as only 21% of the original mass remained after one week.
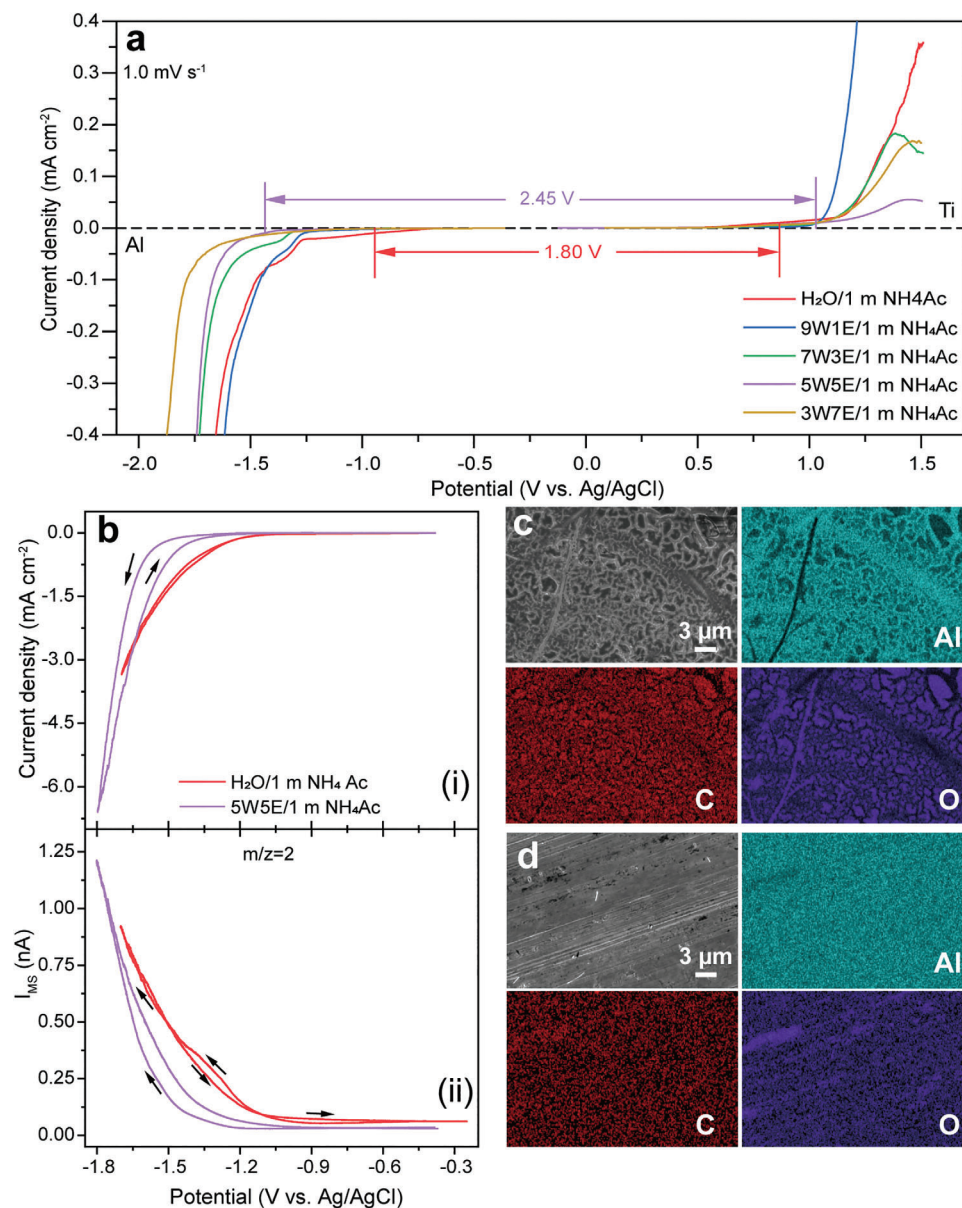
To examine the ESW of the electrolytes, linear sweep voltammetry (LSV) was performed as presented in **Figure 2a**. The ESW could be substantially expanded by EG addition. For example, the ESW of H_2O/1 m NH_4Ac is only 1.80 V while it is significantly extended to 2.45 V in case of 5W5E/1 m NH_4Ac and 3W7E/1 m NH_4Ac (considering 10 μA cm^{-2} as the current density threshold for decomposition). As it is clearly noticed, only a minor improve-

ment is observed in terms of anodic stability. In fact, the enlarged ESW mainly arises from the enhanced cathodic stability resulting from the suppression of HER.

To further investigate this aspect, differential electrochemical mass spectrometry (DEMS) measurements were performed on selected electrolyte compositions, i.e., H_2O/1 m NH_4Ac and 5W5E/1 m NH_4Ac. The latter was chosen as the optimum composition considering the absence of freezing point down to −100 °C, acceptable conductivity and large ESW. An Al-sputtered fluorinated ethylene-propylene (FEP) membrane was directly used as working electrode, with the non-sputtered side facing the mass spectrometer chamber, thus allowing the online detection of the gases evolving from the working electrode.[20] H_2 gas release was detected during the cathodic scan of the CV measurements performed in the voltage windows of −1.7–−0.3 V for H_2O/1 m NH_4Ac and −1.8–−0.3 V for 5W5E/1 m NH_4Ac (Figure 2b). At the same potential of −1.5 V versus Ag/AgCl the signal associated with H_2 gas evolution in the H_2O/1 m NH_4Ac (0.46 nA) is much stronger than that in 5W5E/1 m NH_4Ac (0.17 nA), confirming the largely suppressed HER in the latter electrolyte.

CV measurements with similar testing conditions as in DEMS measurements (from 0.3 to −1.8 V, 0.5 mV s^{-1}) were conducted in typical three-electrode (Swagelok-type) cells and, afterwards, the SEM micrographs and EDX mapping were carried out to examine the morphology of the current collector (see Figure 2c,d). The surface of the Al electrode tested in 5W5E/1 m NH_4Ac shows nearly the same flat and uniform morphology as the bare foil (see Figure S5a,b, Supporting Information). On the other hand, the sample cycled in H_2O/1 m NH_4Ac displays a very rough and irregular surface with clear signs of corrosion (Figure 2c). The Al corrosion is most certainly caused by the local pH increase resulting from H_2 evolution. The SEM images of Al foils at lower magnification are shown to demonstrate the homogeneous morphology over a larger area (see Figure S5c,d, Supporting Information). In summary, besides the direct advantage of a largely improved cathodic stability, the addition of EG also helps suppressing Al corrosion due to the decreased rate of hydrogen evolution.[21]

In view of employing this electrolyte in a full ammonium-ion cell, half-cell measurements of anode and cathode materials were first performed in H_2O/1 m NH_4Ac and 5W5E/1 m NH_4Ac electrolytes in three-electrode cells. Commercially available PTCDI was employed as anode material. As shown by the CV in **Figure 3a**, two pairs of main redox peaks are observed during the insertion/de-insertion of NH_4^+, which are associated with the enolation of carbonyl groups in the PTCDI structure.[22] It should be noted that the redox peaks in H_2O/1 m NH_4Ac are narrower and more intense than those recorded in 5W5E/1 m NH_4Ac, which can be explained by the faster kinetics in H_2O/1 m NH_4Ac electrolyte as a result of its higher ionic conductivity. An obvious redox potential was observed as well, both in the first and the following cycle (see Figure S6a, Supporting Information). To rule out any artefact arising from the leakless Ag/AgCl reference electrode, the measurements were repeated using an activated carbon (AC) quasi reference.[23] As evident from Figure S6b (Supporting Information), the redox peaks shift could still be observed. Therefore, such downshift upon EG addition is not caused by the experimental setup, but it may rather be ascribed to the different NH_4^+ activity in the two electrolytes.[1a] Afterwards, the rate performance of PTCDI in the same electrolytes was

**ADVANCED
SCIENCE NEWS**

www.advancedsciencenews.com

**ADVANCED
FUNCTIONAL
MATERIALS**

www.afm-journal.de

Figure 2. a) ESW of various electrolytes determined by LSV. b) Potentiodynamic DEMS measurements (scan rate: 0.5 mV s^{-1}) on a sputtered Al working electrode in H_2O/1 m NH_4Ac and 5W5E/1 m NH_4Ac electrolytes: i) cyclic voltammetry (CV) curves and ii) selected ion (H_2) current. Scanning electron microscope (SEM) images (upper left panels) and energy dispersive X-ray (EDX) mapping of Al foils after CV measurements between 0.3 and −1.8 V for two cycles at a scan rate of 0.5 mV s^{-1} in c) H_2O/1 m NH_4Ac and d) 5W5E/1 m NH_4Ac.

evaluated, as shown in Figure 3b,c. It must be said that the capacity delivered by the PTCDI electrode in H_2O/1 m NH_4Ac is always higher than that in 5W5E/1 m NH_4Ac. However, interestingly, the discharge/charge profiles in H_2O/1 m NH_4Ac show larger polarization than those in 5W5E/1 m NH_4Ac when increasing the current density from 120 to 600 mA g^{-1}. For a more intuitive comparison of the polarization under each current in two electrolytes, differential capacity curves of PTCDI half-cell under different current densities are plotted in Figure S7 (Supporting Information). As it can clearly be seen, the potential of the lowest redox peak in H_2O/1 m NH_4Ac shifted from −0.76 V (120 mA g^{-1}) to −0.87 V (600 mA g^{-1}) while that in 5W5E/1 m NH_4Ac shifted

from −0.90 V to −0.96 V versus Ag/AgCl. In addition, the H_2O/1 m NH_4Ac experienced very fast capacity decay and poor Coulombic efficiency (CE), which are likely linked to HER and corrosion issues previously discussed. In contrast, the electrochemical stability of PTCDI was vastly improved in 5W5E/1 m NH_4Ac, as shown by the long-term galvanostatic charge-discharge (GCD) measurements at the current density of 600 mA g^{-1} (shown in Figure 3d). The PTCDI electrode in 5W5E/1 m NH_4Ac electrolyte maintained 64% of the initial capacity after 5000 cycles, compared to only 29% in case of H_2O/1 m NH_4Ac. More importantly, the half-cell in 5W5E/1 m NH_4Ac electrolyte displayed a largely enhanced CE (99.0% compared to 88.7% in H_2O/1 m NH_4Ac).
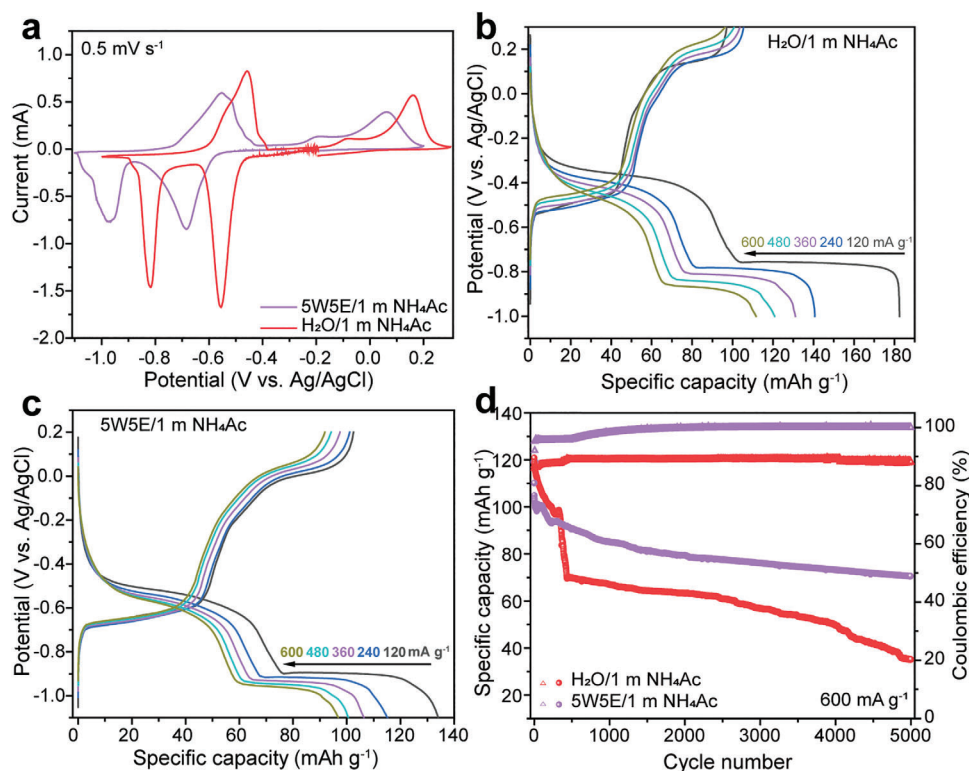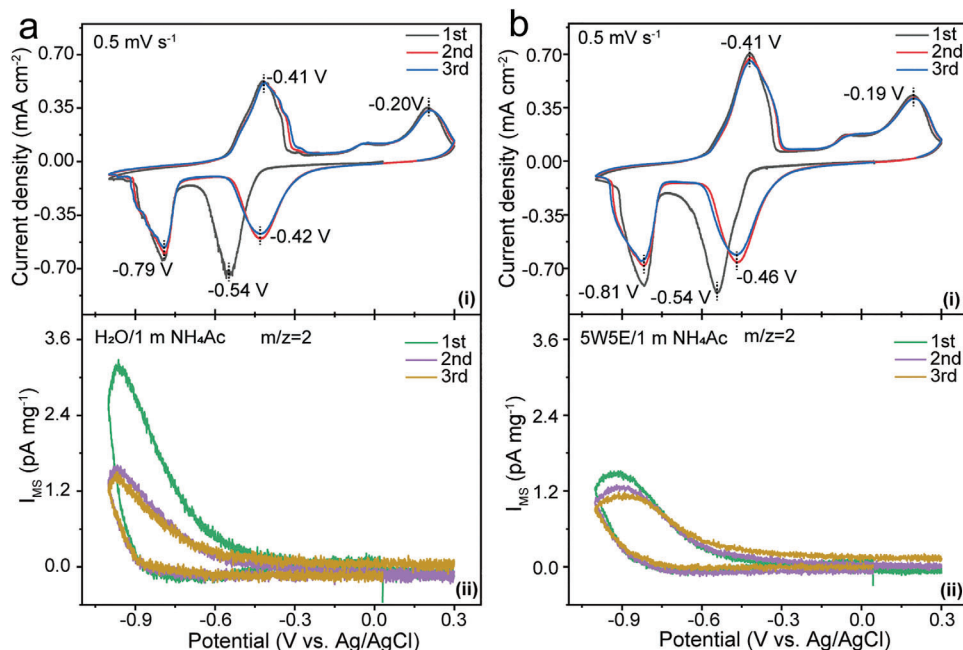
Figure 3. Electrochemical characterization of PTCDI. a) CV curves of PTCDI anode of the first cycle in different electrolytes. GCD curves of PTCDI anode in b) H_2O/1 m NH_4Ac and c) 5W5E/1 m NH_4Ac electrolyte at different current densities. d) Cycling stability of PTCDI anode in H_2O/1 m NH_4Ac and 5W5E/1 m NH_4Ac electrolytes at a current density of 600 mA g^{-1}.

According to previous reports, the capacity fading observed in the initial cycles may result from the slight dissolution of the PTCDI material as well as the side reactions (H_2 evolution, Al_2O_3 reduction and Al corrosion) occurring at negative potentials.[10] In the case of H_2O/1 m NH_4Ac, this results on the redox process at most negative potential to be gradually lost in the initial 500 cycles. In fact, as shown in Figure S8 (Supporting Information), the corresponding plateau shifts outside of the negative cut-off limit due to the increased polarization. On the contrary, the PTCDI electrode maintains the same electrochemical signature in 5W5E/1 m NH_4Ac while the polarization surprisingly decreases. In this case, the capacity loss is less pronounced and associated only with the shortening of the low potential plateau. This means that less time is spent at lower potentials where parasitic reactions occur, thus leading to an increased CE.[24]

To further confirm the stability of the selected electrolytes during half-cell cycling and explore the reason behind the better performance of PTCDI electrode in 5W5E/1 m NH_4Ac, DEMS measurements were again performed, with Al-sputtered FEP membrane or PTCDI coated on Al-sputtered FEP membrane as working electrodes in the voltage windows of −1.0–0.3 V. Figure S9 (Supporting Information) displays the CVs employing Al-sputtered FEP membrane as working electrode and selected ion (H_2) current traces. The detected H_2 gas evolution was nearly negligible in both electrolytes, while the current response of the first cathodic scan in H_2O/1 m NH_4Ac was substantially larger which may be attributed to the reduction of the native Al_2O_3 layer present on the Al-sputtered membrane. Additionally, the current

response in H_2O/1 m NH_4Ac electrolyte during anodic scan was more intensive in all scans, suggesting the Al corrosion. Afterwards, PTCDI coated on Al-sputtered FEP membrane was employed as working electrodes in DEMS cell (see **Figure 4**). The H_2 gas evolution in this case was observed at an earlier onset compared to Figure 2, suggesting that the electrode components (conductive carbon and PTCDI active material) play a role in this process. In our specific case, the mass loading of the electrodes was slightly different (0.44 mg in H_2O/1 m NH_4Ac and 0.90 mg in 5W5E/1 m NH_4Ac). To take this aspect into account, the normalized ion current is considered. Nevertheless, it is quite evident that the H_2 evolution in H_2O/1 m NH_4Ac is much more pronounced, particularly in the first cycle.
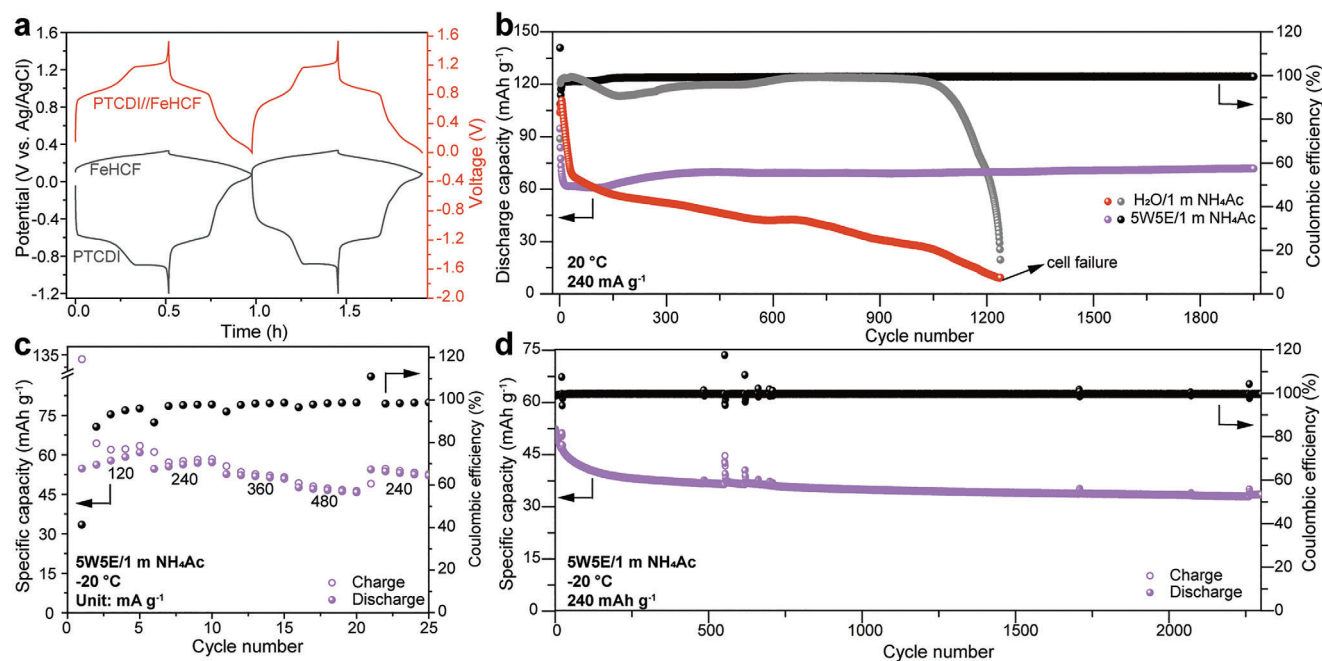
With regards to the cathode material, FeHCF was synthesized according to a simple co-precipitation method previously reported in literature.[25] The X-ray diffraction (XRD) pattern shown in Figure S10a (Supporting Information) confirms the highly crystalline face-centered cubic structure typical of FeHCF. The morphological characterization of the FeHCF powder (seen in Figure S10b, Supporting Information) by SEM imaging reveals well-defined sub-micron particles. FeHCF is an ideal electrode material being low-cost and eco-friendly. However, Fe dissolves in aqueous electrolyte during charge/discharge, resulting in poor electrode's cycling stability.[25,26] CV measurements were conducted in the potential window comprised between −0.3 and 0.6 V (vs Ag/AgCl) as shown in **Figure 5a**. The redox peaks in H_2O/1 m NH_4Ac and 5W5E/1 m NH_4Ac are located at 0.32/0.13 and 0.37/0.08 V, respectively. In 5W5E/1 m NH_4Ac electrolyte

Figure 4. Potentiodynamic DEMS measurements (scan rate: 0.5 mV s^{-1}) on a PTCDI coated sputtered-Al working electrode in a) H_2O/1 m NH_4Ac and b) 5W5E/1 m NH_4Ac electrolytes in the voltage windows of −1.0–0.3 V: i) CV curves and ii) selected ion (H_2) current.
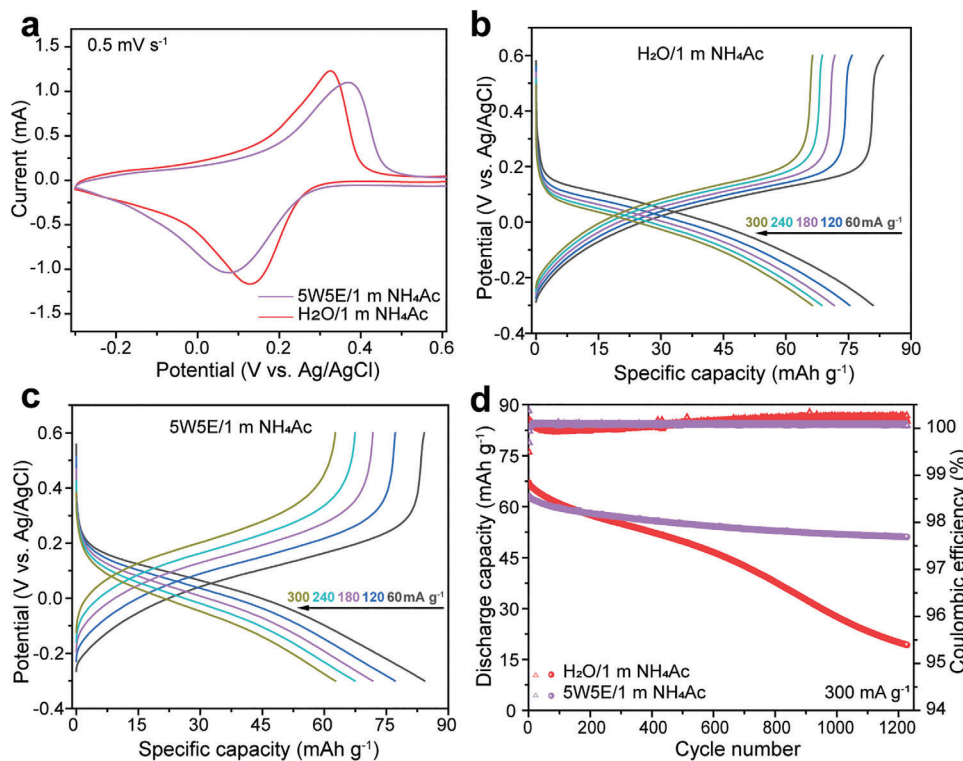
Figure 5. Electrochemical characterization of FeHCF. a) CV curves of FeHCF cathode in different electrolytes. GCD curves of FeHCF cathode in b) H_2O/1 m NH_4Ac and c) 5W5E/1 m NH_4Ac electrolyte at different current densities. d) Cycling stability of FeHCF cathode in H_2O/1 m NH_4Ac and 5W5E/1 m NH_4Ac electrolytes at a current density of 300 mA g^{-1}.

ADVANCED
SCIENCE NEWS
www.advancedsciencenews.com

ADVANCED
FUNCTIONAL
MATERIALS
www.afm-journal.de

Figure 6. Electrochemical performance of PTCDI‖FeHCF full ammonium-ion cells at different working temperatures. a) GCD profiles of PTCDI‖FeHCF full cell with 5W5E/1 m NH$_4$Ac electrolyte, together with individual potential profiles of anode and cathode. b) Long-term cycling performance of PTCDI‖FeHCF full cells in different electrolytes at 20 °C with current density of 240 mA g^{-1}. c) Rate capability test of PTCDI//FeHCF full cell in 5W5E/1 m NH$_4$Ac electrolyte at −20 °C. d) Long-term cycling performance of PTCDI‖FeHCF full cells in 5W5E/1 m NH$_4$Ac electrolyte at −20 °C with current density of 240 mA g^{-1}.

the FeHCF electrode shows larger polarization due to the lower ionic conductivity. However, the specific discharge capacities of FeHCF in 5W5E/1 m NH$_4$Ac are comparable to that in H$_2$O/1 m NH$_4$Ac, as shown by the potential profiles recorded under different current densities (60, 120, 180, 240 and 360 mA g^{-1}) reported in Figure 5b,c. In terms of long-term cycling stability, as shown in Figure 5d, 5W5E/1 m NH$_4$Ac largely outperforms H$_2$O/1 m NH$_4$Ac. The FeHCF cathode cycled in H$_2$O/1 m NH$_4$Ac suffers from rapid capacity decay with only 30% of the initial capacity maintained after 1200 cycles (see Figure S11, Supporting Information). In comparison, the capacity retention in 5W5E/1 m NH$_4$Ac is 81% after 1200 cycles, demonstrating promising cycling stability. As previously mentioned, Fe dissolution is a common issue of FeHCF. To probe this aspect, FeHCF electrodes were immersed into vials containing 1 mL electrolyte for 3 days, as shown in Figure S12 (Supporting Information). The standard aqueous electrolyte without EG exhibited a marked yellowish coloration, suggesting the presence of dissolved Fe^{3+}. Differently, the 5W5E/1 m NH$_4$Ac electrolyte appeared only slightly colored, implying the suppressed iron dissolution.

Finally, PTCDI‖FeHCF full cells were assembled to demonstrate the feasible application of the hybrid electrolyte in a complete device. Before assembly the full cell, the FeHCF cathode was first discharged in a separate half-cell to −0.4 V (vs Ag/AgCl) for the pre-insertion of ammonium ions (current density:30 mA g^{-1}). The typical voltage profile of pre-ammoniation step in half-cell is shown in Figure S13 (Supporting Information). **Figure 6a** displays the first two charge/discharge profiles of the full cell within a voltage range of 0–1.6 V, as well as the individual potential profiles of anode and cathode. As it can be seen, the

voltage profile is largely dominated by the characteristic electrochemical signature of the PTCDI anode, which is also the limiting electrode. Long-term cycling performance at 240 mA g^{-1} in different electrolytes are compared in Figure 6b. The full cell in the hybrid 5W5E/1 m NH$_4$Ac electrolyte showed an initial discharge capacity of 95 mAh g^{-1} based on PTCDI mass, and 77% of this capacity is still retained after 1950 cycles with an average CE of 99.3%. However, the full cell with standard H$_2$O/1 m NH$_4$Ac electrolyte experienced continuous capacity decay, failing after 1230 cycles. The voltage profiles of selected cycles displayed in Figure S14a,b (Supporting Information) provide valuable information on the reasons behind capacity fading. As it can be clearly seen, in both cases the rapid capacity loss observed in the first cycles arises from the loss of the high voltage plateau, which corresponds to the low potential plateau of PTCDI. Afterwards, while 5W5E/1 m NH$_4$Ac allows for a stabilization of the capacity, the performance of the cell with H$_2$O/1 m NH$_4$Ac gradually decayed due to the more severe side reactions and dissolution of the cathode materials. The cell failure after 1230 cycles may be caused by a combination of electrolyte drying out, Al corrosion and Fe dissolution from the cathode.

Unexpectedly, the capacity delivered in the high voltage plateau was partially recovered upon cycling in 5W5E/1 m NH$_4$Ac (Figure S14c, Supporting Information). Presently we do not have a reasonable explanation for this phenomenon, which will have to be investigated in more details in the future. Rate capability tests were also performed in full cell configuration at room temperature, as shown in Figure S15 (Supporting Information). When increasing the current density from 120 to 600 mA g^{-1}, the discharge capacity dropped only slightly from 73 to 66 mAh g^{-1},

**ADVANCED
SCIENCE NEWS**

www.advancedsciencenews.com

**ADVANCED
FUNCTIONAL
MATERIALS**

www.afm-journal.de

testifying the good rate capability of the full cell with the hybrid electrolyte.

The anti-freezing property of the EG containing electrolyte (previously demonstrated by DSC) suggest that cells with 5W5E/1 m NH$_4$Ac may operate in extremely low temperature environments. Therefore, the full cell rate performance was evaluated at $-20\,^\circ$C as displayed in Figure 6c. The discharge capacity at a current density of 120 mA g^{-1} was 61 mAh g^{-1}, corresponding to 64% of the room-temperature performance. A high reversible capacity of 47 mAh g^{-1} is also achieved at a relatively high current density of 480 mA g^{-1}. Additionally, the AAIB with 5W5E/1 m NH$_4$Ac electrolyte presented a cycling stability over 2300 cycles with capacity retention of 66% and average CE of 99.7% (see Figure 6d). Overall, the EG-added electrolyte endows the full cell very encouraging cycling stability because of suppressed side reactions at room temperature as well as at $-20\,^\circ$C.

3. Conclusion

In this work, EG is employed as co-solvent to disrupt the H-bond network in diluted aqueous electrolytes for ammonium-ion batteries. It is demonstrated that, by suppressing HER, the ESW of the electrolyte can be expanded up to 2.45 V. Additionally, further side reactions such as corrosion of the Al current collector and active material dissolution are substantially inhibited. Ultimately, EG-containing electrolytes enable superior electrochemical performance of FeHCF‖PTCDI full cells, both at room temperature and, most remarkably, at $-20\,^\circ$C.

4. Experimental Section

Materials and Electrolytes: The electrolyte concentration was either 1 m NH$_4$Ac (VWR chemicals, ACS, Reag. Ph. Eur.), or 10 m NH$_4$Ac. Different water (Milli-Q) to EG (VWR chemicals, Reag. Ph. Eur.) volume ratios were studied, referred as 9W1E, 7W3E, 5W5E, and 7W3E. Commercial PTCDI powder was supplied by Alfa Aesar. FeHCF cathode material was synthesized by a co-precipitation method according to previous literature.[25] First, 1.646 g of K$_3$Fe(CN)$_6$ (Sigma Aldrich) were dissolved in 50 mL Milli-Q water and 1.622 g of anhydrous FeCl$_3$ (VWR chemicals) were dissolved in 100 mL water. Then, the K$_3$Fe(CN)$_6$ solution was added to the FeCl$_3$ solution drop by drop, while stirring. The green solution was kept stirring for 6 h at room temperature until the product precipitated. Finally, the resulting green powder was centrifuged, washed three times with water and dried 50 °C at in vacuum overnight for further use.

Characterizations Method: The physical properties of the various electrolytes were studied by multiple techniques. IR spectra of the electrolytes and solvents were acquired by means of a MAGNA FTIR-750-Nicolet spectrometer. Raman spectra of various electrolytes and solvents were obtained via a Renishaw InVia confocal Raman microscope with a 532 nm excitation laser. NMR (^{1}H NMR) spectroscopy measurements at room temperature were performed using a Bruker Avance. The ionic conductivity of the electrolytes was determined in sealed glass cells with two platinum electrodes (cell constant of 1.0 ± 0.1 cm), which were connected to a Bio-Logic conductivity meter. The temperature was varied by means of a Peltier stage from -30 to 40 °C with a step size of 10 °C. DSC experiments were conducted via a TA Instruments Q2000 analyzer with a temperature range from -100 to 40 °C. The electrolytes were first cooled down from 40 to -100 °C, and afterwards heated up to 40 °C at a rate of 5 °C min^{-1}. The morphology and compositions of commercial PTCDI powder, synthesized FeHCF material and Al foils were characterized by SEM (ZEISS Crossbeam XB340) equipped with an EDX detector. In addition, the crystallographic properties of the electrode material were studied with a Bruker D8 Advance diffractometer. The solubility test of FeHCF in different electrolytes was performed by immersing the FeHCF electrodes in 1 mL electrolyte solution for 3 days.

Electrochemical Characterization: The electrochemical window of the electrolytes was determined by LSV in three-electrodes Swagelok-type cells at a scan rate of 1.0 mV s^{-1}. Ti/Al disks with a diameter of 12 mm were used as working electrode for the anodic/cathodic scan. AC pellets with a diameter of 12 mm as counter electrode were homemade, composed of 15% polytetrafluorethylen (60 wt% dispersion in H$_2$O, Sigma–Aldrich) and 85% AC (YP50 from Kuraray). Reference electrodes were either leakless Ag/AgCl electrode or AC pellets with a diameter of 8 mm. The electrode compositions were: 70 wt% of active material (either FeHCF or PTCDI), 20 wt% conducting carbon (Super C65) and 10 wt% PVDF binder. The cathode materials were casted on Ti foils and anodes materials were coated on Al foil. The assembled half cells were constituted of FeHCF or PTCDI as working electrodes, AC pellets as counter electrode and Ag/AgCl or AC pellets as reference electrodes. GCD measurements were carried out on a battery tester (MACCOR, 4000). All CVs were performed using a programmable potentiostat (VMP-3 Biologic Science) with a scan rate of 0.5 mV s^{-1}. Before assembling full cells, the FeHCF cathode was first discharged to -0.4 V (vs Ag/AgCl) for the pre-insertion of ammonium ions using a current density of 30 mA g^{-1} in half-cell. PTCDI‖FeHCF full cells were assembled in 2032-coin cell configuration for long-term stability tests. A three-electrode cell setup (FeHCF as working electrode, PTCDI as counter electrode and Ag/AgCl as reference electrode) was utilized to acquire the charge–discharge profiles of the full cell and the individual electrodes. In all three-electrode systems, the separators between the working and counter electrode were GF/A (Whatman) and the separators for the reference electrodes were GF/D (Whatman). All the cells were tested at 20 °C or -20 °C.

DEMS Measurements: For DEMS measurements, a leakless Ag/AgCl was used as reference electrode and AC coated on both sides of Al foil was utilized as counter electrode. The DEMS set-up was the same as reported in ref.[20,27], with a quadrupole mass spectrometer (Pfeiffer Vacuum, QMS 422) and the potential control was achieved by an electrochemical workstation (Pine Instruments, AFRDE 5). For obtaining the gas evolution when determining the ESW of different electrolytes, 50 nm Al sputtered on a 50 µm thick FEP film (Bohlender, Bola) with a diameter of 12 mm was used as the working electrode. It should be mentioned that the aluminum oxide could significantly suppress the HER.[28] In order to exclude any influence from the surface layer, since it was not possible to entirely define its properties when using sputtered Al, it was decided to use the same working electrode in both electrolytes, i.e., H$_2$O/1 m NH$_4$Ac and 5W5E/1 m NH$_4$Ac. In addition, cathodic scan was first carried out to eliminate the influence of such oxide on the potential shift, since it could be partly reduced at low potentials. In addition, the PTCDI slurry was casted on 50-nm thick Al foil sputtered on the FEP film, with a mass loading of $\approx$0.5–1.0 mg cm^{-2} and then dried at 80 °C. Afterwards, the working electrodes with PTCDI material was cut into 12 mm disks. All the cell components were assembled in a modified Swagelok T-cell body. The amount of the electrolytes in DEMS measurements was ca. 0.5 mL for each measurement.

Supporting Information

Supporting Information is available from the Wiley Online Library or from the author.

Acknowledgements

Conflict of Interest

The authors declare no conflict of interest.

Data Availability Statement

The data that support the findings of this study are available from the corresponding author upon reasonable request.

[1] a) L. M. Suo, O. Borodin, T. Gao, M. Olguin, J. Ho, X. L. Fan, C. Luo, C. S. Wang, K. Xu, *Science* **2015**, *350*, 938; b) Z. Huang, Y. Hou, T. Wang, Y. Zhao, G. Liang, X. Li, Y. Guo, Q. Yang, Z. Chen, Q. Li, L. Ma, J. Fan, C. Zhi, *Nat. Commun.* **2021**, *12*, 3106.

[2] a) J. C. Chen, S. L. Lei, S. X. Zhang, C. Y. Zhu, Q. Y. Liu, Z. W. Zhang, S. J. Wang, Y. C. Shi, L. W. Yin, R. T. Wang, *Adv. Funct. Mater.* **2023**, *33*, 2215027; b) Y. Wang, T. R. Wang, S. Y. Bu, J. X. Zhu, Y. B. Wang, R. Zhang, H. Hong, W. J. Zhang, J. Fan, C. Y. Zhi, *Nat. Commun.* **2023**, *14*, 1828; c) G. A. Elia, K. Marquardt, K. Hoeppner, S. Fantini, R. Y. Lin, E. Knipping, W. Peters, J. F. Drillet, S. Passerini, R. Hahn, *Adv. Mater.* **2016**, *28*, 7564.

[3] a) Z. W. Guo, J. H. Huang, X. L. Dong, Y. Y. Xia, L. Yan, Z. Wang, Y. G. Wang, *Nat. Commun.* **2020**, *11*, 959; b) X. Wu, Y. Qi, J. J. Hong, Z. Li, A. S. Hernandez, X. Ji, *Angew. Chem. Int. Ed.* **2017**, *56*, 13026.

[4] a) J. Han, A. Varzi, S. Passerini, *Angew. Chem. Int. Ed.* **2022**, *61*, 202115046; b) R. Zheng, Y. Li, H. Yu, X. Zhang, Y. Ding, L. Yan, Y. Li, J. Shu, B. L. Su, *Angew. Chem. Int. Ed.* **2023**, *62*, 202301629.

[5] Y. Wang, S. F. Kuchena, *Acs Omega* **2022**, *7*, 33732.

[6] a) J. Han, M. Zarrabeitia, A. Mariani, M. Kuenzel, A. Mullaliu, A. Varzi, S. Passerini, *Adv. Mater.* **2022**, *34*, 2201877; b) Y. Wang, T. Wang, D. Dong, J. Xie, Y. Guan, Y. Huang, J. Fan, Y.-C. Lu, *Matter* **2021**, *5*, 162.

[7] a) L. Chen, W. L. Sun, K. Xu, Q. Y. Dong, L. Zheng, J. Wang, D. R. Lu, Y. B. Shen, J. Y. Zhang, F. Fu, H. B. Kong, J. Q. Qin, H. W. Chen, *Acs Energy Lett.* **2022**, *7*, 1672; b) J. J. Holoubek, H. Jiang, D. Leonard, Y. Qi, G. C. Bustamante, X. Ji, *Chem. Commun.* **2018**, *54*, 9805; c) L. Y. Du, S. S. Bi, M. Yang, Z. W. Tie, M. H. Zhang, Z. Q. Niu, *Proc. Natl. Acad. Sci. USA* **2022**, *119*, 2214545119.

[8] a) T. Liang, R. Hou, Q. Dou, H. Zhang, X. Yan, *Adv. Funct. Mater.* **2021**, *31*, 2006749; b) L. Suo, O. Borodin, Y. Wang, X. Rong, W. Sun, X. Fan, S. Xu, M. A. Schroeder, A. V. Cresce, F. Wang, C. Yang, Y.-S. Hu, K. Xu, C. Wang, *Advanced Energy Materials* **2017**, *7*, 1701189.

[9] N. Agmon, *Chem. Phys. Lett.* **1995**, *244*, 456.

[10] Z. Tian, J. Yin, T. Guo, Z. Zhao, Y. Zhu, Y. Wang, J. Yin, Y. Zou, Y. Lei, J. Ming, O. Bakr, O. F. Mohammed, H. N. Alshareef, *Angew. Chem. Int. Ed.* **2022**, *61*, 202213757.

[11] Y. Shen, B. Liu, X. Liu, J. Liu, J. Ding, C. Zhong, W. Hu, *Energy Stor. Mater.* **2021**, *34*, 461.

[12] J. Xie, Z. Liang, Y.-C. Lu, *Nat. Mater.* **2020**, *19*, 1006.

[13] Y. Matsuki, M. Iwamoto, K. Mita, K. Shigemi, S. Matsunaga, S. Oiki, *J. Am. Chem. Soc.* **2016**, *138*, 4168.

[14] a) A. Tron, S. Jeong, Y. D. Park, J. Mun, *ACS Sustain. Chem. Eng.* **2019**, *7*, 14531; b) X. Li, H. Wang, H. Sun, J. Li, Y.-N. Liu, *Acs Appl. Energy Mater.* **2021**, *4*, 12718; c) N. Wang, Y. Yang, X. Qiu, X. Dong, Y. Wang, Y. Xia, *ChemSusChem* **2020**, *13*, 5556.

[15] a) N. Chang, T. Li, R. Li, S. Wang, Y. Yin, H. Zhang, X. Li, *Energy Environ. Sci.* **2020**, *13*, 3527; b) R. M. Kumar, P. Baskar, K. Balamurugan, S. Das, V. Subramanian, *J. Phys. Chem. A* **2012**, *116*, 4239.

[16] B. Yang, P. Ren, L. Xing, C. Sun, Z. Men, *J. Phys. Chem. Lett.* **2023**, *14*, 1641.

[17] Y. Wang, Z. Wang, W. K. Pang, W. Lie, J. A. Yuwono, G. Liang, S. Liu, A. M. Angelo, J. Deng, Y. Fan, K. Davey, B. Li, Z. Guo, *Nat. Commun.* **2023**, *14*, 2720.

[18] S. Kang, A. Singh, K. G. Reeves, J.-C. Badot, S. Durand-Vidal, C. Legein, M. Body, O. Dubrunfaut, O. J. Borkiewicz, B. Tremblay, C. Laberty-Robert, D. Dambournet, *Chem. Mater.* **2020**, *32*, 9458.

[19] a) G. Wu, X. Chen, X. Meng, L. Wang, X. Sun, M. Wang, H. Sun, H. Zhang, J. Qin, D. Zhu, *Energy & Fuels* **2021**, *35*, 12119; b) J. Wang, Y. Huang, B. Liu, Z. Li, J. Zhang, G. Yang, P. Hiralal, S. Jin, H. Zhou, *Energy Storage Mater.* **2021**, *41*, 599.

[20] J. Han, M. Zarrabeitia, A. Mariani, Z. Jusys, M. Hekmatfar, H. Zhang, D. Geiger, U. Kaiser, R. J. Behm, A. Varzi, S. Passerini, *Nano Energy* **2020**, *77*, 105176.

[21] G. A. Zhang, L. Y. Xu, Y. F. Cheng, *Electrochimica Acta* **2008**, *53*, 8245.

[22] Z. Zhang, Y. Zhu, M. Yu, Y. Jiao, Y. Huang, *Nat. Commun.* **2022**, *13*, 6489.

[23] X. Liu, G. A. Elia, S. Passerini, *J. Power Sources Adv.* **2020**, *2*, 100008.

[24] L. Droguet, A. Grimaud, O. Fontaine, J.-M. Tarascon, *Adv. Energy Mater.* **2020**, *10*, 2002440.

[25] S. Li, M. Xia, C. Xiao, X. Zhang, H. Yu, L. Zhang, J. Shu, *Dalton Trans.* **2021**, *50*, 6520.

[26] H. Y. Asl, A. Manthiram, *Science* **2020**, *369*, 140.

[27] Z. Jusys, M. Binder, J. Schnaidt, R. J. Behm, *Electrochimica Acta* **2019**, *314*, 188.

[28] Z. Hou, X. Zhang, H. Ao, M. Liu, Y. Zhu, Y. Qian, *Mater. Today Energy* **2019**, *14*, 100337.